Polymer Chemistry

ROYAL SOCIETY OF CHEMISTRY

PAPER

View Article Online
View Journal | View Issue

Cite this: *Polym. Chem.*, 2024, **15**, 4763

Protic poly(diallylmethylammonium) poly(ionic liquid) proton exchange membranes with low fluorine content†

Yuliana Pairetti,[a] Antonela Gallastegui,*[a] Zaneta Wojnarowska,[b] Marian Paluch,[b] Ilaria Abdel Aziz,[a] Nerea Casado,[a,c] Luke A. O'Dell,[d] Maria Forsyth[c,d] and David Mecerreyes *[a,c]

Proton exchange membranes (PEMs) are being studied as a key component to extend and improve green hydrogen technologies. One important issue nowadays is the need for reducing the amount of poly-fluoro alkyl substances (PFSA)s in materials employed in renewable energy devices due to their high toxicity. In the present work, we introduce a family of PFSA-free protic poly(ionic liquid)s based on cationic poly(diallylmethylammonium) (PolyDAMAH) and sulfonamides such as bis(trifluorosulfonyl)imide (TFSI) and bis(fluorosulfonyl)imide (FSI) as counter-anions. The synthesis was carried out in a three step procedure, first synthesizing the protic diallylammonium chloride monomer, then thermal radical polymerization and finally anion exchange of the chloride anion by the specified sulfonamide anions. The protic PolyDAMAH showed apparent molecular weights between 30 K and 40 K and glass transition values of 39 and 52 °C, respectively, for both homopolymers and high thermal stability up to 250 °C. From solid state NMR studies it was found that the FSI^- anion may allow a faster proton and anion mobility when compared to the $TFSI^-$ anion in dry and humid states. To find the best match, blending protic poly(ionic liquid)s with $TFSI^-$ and FSI^- anions improved the mechanical characteristics of the membranes, while maintaining low water uptake and high ionic conductivity. The optimized PolyDAMAH membranes were characterized by dielectric and mechanical relaxation measurements and showed more than six orders of magnitude decoupling of the ion dynamics from the mechanical relaxation. An ionic conductivity of 1.2×10^{-3} S cm^{-1} at 100 °C and 75% relative humidity with the storage modulus higher than 2.2×10^{-5} Pa at 80 °C was obtained for the optimized blend, making this a promising material to be employed as proton exchange membranes for fuel cells at intermediate temperatures.

Received 3rd October 2024,
Accepted 30th October 2024

DOI: 10.1039/d4py01099j

rsc.li/polymers

Introduction

Industrialization, population expansion and technological advancements are steadily escalating the global energy demand.[1] Over the years, reliance on fossil fuel reserves to satisfy humanity's energy requirements has led to their gradual depletion. Hence, there has been a global research emphasis on harnessing renewable energy sources and enhancing energy efficiency.[2] Among these alternatives, proton exchange membrane fuel cells (PEMFCs) have emerged as viable substitutes for internal combustion engines in recent times and are promising candidates as the power source for next-generation transportation and portable applications.[3,4] PEMFCs convert chemical energy into electrical energy using hydrogen as the fuel. As the heart, the proton exchange membrane is the driving force behind the fuel cell's operation, allowing the transfer of protons between the electrodes while withstanding the harsh operating conditions.[5]

Proton exchange membranes (PEMs) are the key component of the FC efficiency and represent approximately 30% of the material cost.[6] Perfluorosulfonic acid polymers (PFSAs), like Nafion, the standard gold material employed nowadays, demonstrate crucial characteristics for PEMs, including high proton conductivity, outstanding mechanical resilience, and robust chemical stability.[6–8] However, Nafion membranes must operate at low temperatures (<100 °C) to avoid membrane dehydration which leads to significant reduction in conductivity. Moreover, as high-fluorine and poly-fluoroalkyl sub-

[a]*POLYMAT, University of the Basque Country UPV/EHU, Avenida Tolosa 72, Donostia-San Sebastian, 20018 Gipuzkoa, Spain. E-mail: david.mecerreyes@ehu.eus*
[b]*Institute of Physics, University of Silesia, Uniwersytecka 4, Katowice 40-007, Poland*
[c]*IKERBASQUE, Basque Foundation for Science, Bilbao, Spain*
[d]*Institute for Frontier Materials and ARC Industry Training Transformation Centre for Future Energy Storage Technologies (StorEnergy), Deakin University, Burwood, Victoria 3125, Australia*

† Electronic supplementary information (ESI) available. See DOI: https://doi.org/10.1039/d4py01099j

stance (PFSA) content polymers, they contribute to the complexity of the manufacturing process, resulting in increased costs and the generation of environmentally harmful byproducts.

Capable of operating at temperatures exceeding 100 °C, high-temperature proton exchange membrane fuel cells (HT-PEMFCs) present several significant benefits, including simplified heat and water management systems, enhanced electrode material reaction kinetics, and increased tolerance of platinum catalysts to carbon monoxide poisoning.[8,9] The polybenzimidazole (PBI) matrix infused with phosphoric acid has emerged as one of the most prominent polymer electrolytes for high-temperature PEMFCs due to its good combination of properties between proton conductivity and manageability.[10,11] However, optimal proton conductivity in phosphoric acid-doped PBI membranes typically requires high phosphoric acid loadings.[12] Nonetheless, a significant drawback arises from the auto dehydration of phosphoric acid at elevated temperatures, leading to the formation of oligomers with reduced conductivity and Pt poisoning resulting from the strong adsorption of phosphoric acid on the Pt catalyst surface.[13,14] On the other hand, sulfonated poly(ether ether ketone) (SPEEK) is an aromatic polymer that has been extensively investigated as a high-performance and cost-effective polymer electrolyte membrane for commercial fuel cell applications. The proton mobility and conductivity of SPEEK depend upon the degree of sulfonation; higher sulfonation enhances ionic conductivity but reduces mechanical strength due to increased water uptake characteristics of the resulting membrane. To overcome this issue, protic ionic liquids, a subclass of ionic liquids (ILs) characterized by the presence of labile protons that usually endow them with unique proton activity, can be added to enhance proton mobility.[15–18] Protic ionic liquids have gained significant attention recently due to their high proton conductivity around 10^{-2} S cm^{-1} at temperatures above 100 °C and under anhydrous conditions.[19–21] Additionally, they offer high thermal and electrochemical stability, with degradation temperatures around 200–300 °C and a broad operational electrochemical window.[22,23] In the case of SPEEK materials, when mixed with a protic IL, a clear proton conductivity boost can be seen in composite SPEEK PEMs without requiring hydration. Consequently, the success of these membranes is limited by the affinity or compatibility of the protic IL and the sulfonated polymer, the preparation of the composite membrane and the leaching effect, which is a big known issue.[22,24] Among the different protic ILs, imidazolium and in particular pyrrolidinium ones are the preferred ones due to their high ionic conductivity and electrochemical stability.[31–33]

The polymeric version of the ILs known as protic poly(ionic liquid)s are emerging as a favored alternative material for PEMs. This is due to their high protic conductivity, non-leaching, good compatibility with protic ionic liquids and wide electrochemical stability, along with desirable properties of polymer materials, such as mechanical stability and flexibility.[25–28] As an example, Isik *et al.* synthesized anionic protic poly(ionic liquid)s employing commercial phosphonium counter-cations achieving a high dry ionic conductivity of 2×10^{-4} S cm^{-1} at 150 °C.[29] Another noteworthy example is the recent research conducted by Huang *et al.*, wherein they enhanced the ionic conductivity of an anionic polystyrene-type protic poly(IL) by integrating the protic IL with a similar chemical structure to the polymer. The dry protic poly(IL) presented a low ionic conductivity of 1×10^{-7} S cm^{-1} at 100 °C, while with an addition of 60 wt% of protic IL, the conductivity increased to 7×10^{-3} S cm^{-1} at the same temperature.[30] More recent works have focused on the development of cationic protic polyILs as hosts of protic ILs. As examples, Wang *et al.* and Karlsson *et al.* recently developed protic poly(IL) membranes functionalized with imidazole and doped with different acids.[34,35] Similarly, Aslan *et al.* showed the development of a triazole and triflic acid blend as proton conductors obtaining very interesting results.[36]

Among the previous studies, only a few have focused on investigating the overall properties and performance of neat protic cationic poly(ionic liquid)s without molecular protic IL additives, aiming to rival the most desirable characteristics of proton exchange membranes for FCs. In our recent research, we showed the synthesis of protic poly(diallylmethyl ammonium) proton conducting membranes primarily through photopolymerization.[37] This study explored how the presence of a proton in the stable pyrrolidinium cationic polymeric backbone and the use of different anion chemistries influenced the material properties, with an eye toward potential applications in PEMFCs. The protic poly(DAMAH$^+$X$^-$) membranes exhibited notable ionic conductivity and proton activity, which varied depending on the anion employed. Among the protic polymers, poly(DAMAH$^+$MsO$^-$), containing the sulfonated mesylate anion, achieved comparable ionic conductivity results to Nafion 112 under the same and varying relative humidity conditions at 80 °C and superior conductivity at 120 °C without the need for humidification. Unfortunately, these protic membranes exhibited poor mechanical properties and manageability mainly due to their hydrophilicity and crosslinked nature.

In this work, we show the synthesis and characterization of low-fluorine content protic poly(ionic liquid)s based on poly(diallylmethylammonium) bis(fluorosulfonyl)imide, poly(DAMAH$^+$FSI$^-$), and bis(trifluorosulfonyl)imide, poly(DAMAH$^+$TFSI$^-$). The membrane forming ability of the homopolymers and blended protic poly(ionic liquid)s was studied with respect to proton mobility, swelling characteristics and ionic conductivity. Furthermore, the mechanical and chemical structure-dynamic properties of the protic poly(ionic liquid) membrane were investigated in detail aiming at optimizing its properties as PFSA free proton exchange membranes.

Experimental section

Materials

Diallylmethylamine (DAMA, 98%), sorbitan sesquiolate (Span 83) and thermal initiator 2,2′-azobis(2-methylpropionamidine)

dihydrochloride (AIBA, 98%) were purchased from Thermo Fisher. Lithium bis(fluorosulfonyl)imide (LiFSI, 99%) and lithium bis(trifluoromethanesulfonyl)imide (LiTFSI, 99%) were obtained from Solvionic. Hydrochloric acid (HCl, 37 wt% in H_2O) was acquired from Thermo Fisher. Isoparaffin L was bought from Scharlab. Acetonitrile (ACN) was obtained from Honeywell. MilliQ water was employed during the work. All the purchased reagents were of analytical grade and employed without further purification.

Inverse emulsion polymerization of protic DAMAH$^+$Cl$^-$

The DAMAH$^+$Cl$^-$ protic monomer was prepared by reacting diallyl methylamine (DAMA) and hydrochloric acid (HCl) in a 1 : 1 molar ratio following a procedure reported previously.[37] The free radical thermal polymerization of protic DAMAH$^+$Cl$^-$ was initiated with 2,2′-azobis(2-methylpropionamidine)dihydrochloride (AIBA). The reaction was carried out *via* inverse emulsion polymerization in water where a mixture of DAMAH$^+$Cl$^-$, AIBA (6.5 wt% with respect to the monomer), and water (100 wt% with respect to the monomer) was added dropwise to an organic solution of two surfactants, Span 83 (15.5 wt% with respect to the monomer) and Tween 40 (23 wt% with respect to the monomer), dissolved in the organic solvent, Isopar L which is a mixture of highly pure saturated aliphatic hydrocarbons (1.7 times monomer's weight). After homogenizing the emulsion, the solution underwent deoxygenation for 30 min and reacted overnight under stirring at 65 °C. In order to eliminate the surfactants and possible remaining monomer and initiator, the polymer was precipitated in acetone, a step repeated three times to ensure polymer's purity. The following and the last step was the typical anion exchange reaction, poly(DAMAH$^+$Cl$^-$) was dissolved in water and lithium bis(fluorosulfonyl)imide (LiFSI) was added in a molar ratio 1 : 1.2 incrementally with stirring to exchange the anion Cl$^-$ and formed the new protic poly(ionic liquid), poly(DAMAH$^+$FSI$^-$), as a white precipitate. The precipitate was redissolved in acetone and dried in an oven at 60 °C for 24 h.

Characterization methods

^{1}H nuclear magnetic resonance (^{1}H NMR). NMR spectra of the monomer DAMAH$^+$Cl$^-$ and the polymer poly(DAMAH$^+$Cl$^-$) were acquired using a Bruker Avance DPX 300 spectrometer operating at 300.16 MHz, employing deuterated dimethyl sulfoxide (DMSO) as the solvent at room temperature. Pulsed field gradient NMR experiments were conducted on a Bruker Avance III 300 MHz spectrometer equipped with a Diff50 probe. A stimulated echo pulse sequence was employed, with standard parameters including 2 ms gradient pulses, a 20 ms diffusion period, and a maximum gradient strength of 3000 G cm^{-1}. Signal attenuation was analyzed using the Stejskal–Tanner equation within the TopSpin software suite.

Fourier transform infrared (FTIR). FTIR spectra were acquired utilizing a Bruker Alpha II spectrophotometer equipped with a platinum Attenuated Total Reflectance (ATR) module featuring a diamond window, covering the spectral range from 4000 cm^{-1} to 500 cm^{-1}. Spectral acquisition consisted of 32 scans at a resolution of 4 cm^{-1}.

Thermogravimetric analysis (TGA). The thermal stability of the samples was examined *via* TGA using a TGA Q500 instrument from TA Instruments. The samples underwent heating at a rate of 10 °C min^{-1} under a nitrogen (N_2) atmosphere, spanning from room temperature to 800 °C.

Differential scanning calorimetry (DSC). DSC was utilized to determine the glass transition temperature (T_g) of both pure homopolymers and their blends. This analysis was run using a DSC Q2000 instrument from TA Instruments. Before testing, all samples were dried overnight at 60 °C under vacuum and then sealed in hermetic pans. DSC scans were performed at a heating rate of 10 °C per minute over a temperature range spanning from −80 °C to 150 °C. The T_g extrapolation was performed during the second heating cycle to account for any prior thermal history of the samples.

Solid-state NMR and pulse field gradient (PFG) NMR. A Bruker Avance III 300 MHz wide-bore NMR spectrometer operating at an ^{1}H Larmor frequency of 300.13 MHz was used for static solid-state NMR measurements. The sample temperatures were calibrated with lead nitrate using the method described in previous studies.[18]

The ^{1}H diffusion coefficients of dry and humid protic homopolymers were obtained using PFG-NMR on a Bruker Avance III 300 MHz wide-bore NMR spectrometer equipped with a 5 mm Diff 50 pulse field gradient probe. The samples were sealed into a 4 mm solid-state NMR rotor inside the glove-box in the case of anhydrous samples, which were then inserted into a standard 5 mm NMR glass tube for experiments. A stimulated echo pulse sequence was used to measure both ^{1}H diffusion coefficients. The typical gradient pulse duration was 10 ms, and the gradient strength was varied in log scale, 32 steps between 1 and 2500 G cm^{-1}. The diffusion time was 100 ms, the recycle delay was 2 s, and 16 scans were accumulated for ^{1}H spectra. The diffusion coefficients were calculated from the Stejskal–Tanner equation and were used to determine the diffusion behavior of the protic cation backbone species, respectively.[38]

Size exclusion chromatography (SEC). A 1200 Infinity gel permeation chromatograph (GPC, Agilent Technologies) was used to determine the M_w and $Đ$ of the protic poly(ionic liquid). The chromatograph was equipped with an integrated IR detector, a PLgel 5 mm MIXED-D column and a PLgel guard column (Agilent Technologies). The eluent was a 0.1 M Li(CF$_3$SO$_2$)$_2$N solution in THF and the flow rate was of 1.0 mL min^{-1} at 50 °C.

Humidity uptake. The moisture absorption of membranes was assessed at three distinct relative humidities: 30%, 50%, and 75%, over time. After drying in an oven for 24 h at 60 °C under vacuum conditions, the materials were exposed to varying humidities for a duration of time and subsequently weighed. This procedure was repeated until a consistent weight was attained. The swelling percentage was determined using the following formula:

$$\%_{WU} = \frac{W_1 - W_0}{W_0} \times 100$$

where, W_1 is the weight of the sample after taking water; W_0 is the weight of the sample before taking water.

Each point of the humidity uptake curve belongs to the average of three individual determinations.

Electrochemical impedance spectroscopy (EIS). EIS was employed to determine the ionic conductivity of dried pure homopolymers and its blends in an Autolab 302 N potentiostat galvanostat at different temperatures (100–30 °C) with an equilibration time of 20 min at each temperature before measurements to assure equilibration. The samples were placed between two stainless steel electrodes (surface area of 0.5 cm^2) and the thickness was kept constant using a 150 μm PTFE spacer. The measurements were obtained in the range between 300 kHz and 1 Hz, with a perturbation amplitude of 20 mV.

The ionic conductivity obeys the Arrhenius equation $\sigma = \sigma_o^{(-E_a/RT)}$ (where σ_o is a pre-exponential factor, E_a is the activation energy, R is the gas constant and T is the temperature in K) yielding a straight line when plotted as the natural logarithm *versus* reciprocal temperature.[39]

Dynamic mechanical analysis (DMA). DMA was performed using a TA Instruments DMA Q800 apparatus. Scans were conducted from 0.01 to 35 Hz at 25 and 80 °C. Mechanical properties were also evaluated using a digital force gauge ZP-500N; Imada Inc. with a load cell at a drawing speed of 10 mm min^{-1}. Measurements were carried out under ambient conditions with film specimens (25 mm (length) × 10 mm (width) × 0.5 mm (thickness)), and Young's modulus and elongation were calculated as an average of at least three samples.

Dielectric measurements. The dielectric measurements in a wide frequency range of 10^{-2} Hz to 10^7 Hz were performed at ambient pressure using a Novo-Control GMBH Alpha dielectric spectrometer. The same stainless steel electrodes (diameter = 15 mm) with a fixed distance (0.1 mm) provided by the quartz ring were used for the studied polyILs. During the measurements, the temperature was controlled using a Novocool system with a nitrogen gas cryostat with an accuracy of 0.1 K.

Mechanical measurements. The mechanical measurements were performed employing an ARES G2 rheometer. In the supercooled liquid region, aluminum parallel plates of diameter 4 mm were used. The rheological experiments were performed in the frequency range from 0.1 to 100 rad s^{-1} (10 points per decade) with strain equal to 0.01% in the vicinity of the liquid glass transition.

Results and discussion

Synthesis and characterization of protic poly (diallylammonium) sulfonamide poly(ionic liquid)s

This work details an easy-to-make synthesis route to a polymerizable protic ionic liquid, starting with the synthesis of the protic monomer by a simple step: an acid–base reaction between diallyl methylamine (DAMA) and hydrochloric acid (HCl) in a 1 : 1 molar ratio. Following the procedure previously reported[37] the acid was incrementally added to the DAMA base with continuous stirring, employing an ice bath due to the highly exothermic nature of the reaction. The reaction proceeded for 24 h during which the protonation of DAMA occurred as shown in Scheme 1a (step 1), resulting in the desired protic ionic liquid monomer: $DAMAH^+Cl^-$. To verify the success of the reaction, ^1H NMR analysis in *d*-DMSO was performed, revealing the presence of the proton with a distinctive signal in the range between 11.5 and 11.7 ppm observed in Scheme 1b. The integration of all signals was verified and a comparison between the base, acid and the synthesized protic monomer ^1H NMR spectrum can be observed in Fig. S1a,† where a clear shifting of the acid proton is shown between the $DAMAH^+Cl^-$ monomer spectrum and the HCl one. Going back to Scheme 1b, vinylic signals can be observed between 5 and 6 ppm, and extra signals belonging to the methylenes next to the nitrogen can be observed at around 3.7 ppm. Proton signals from vinyls, methylenes and even methyl groups suffered an up-field shifting, as appreciated for the DAMA spectrum in Fig. S1a† when compared to the protic $DAMAH^+Cl^-$ monomer once formed, confirming this way the successful synthesis of the protic monomer. As a complementary characterization, FTIR has been performed on the $DAMAH^+Cl^-$ monomer, where the characteristic peaks of the protic compound are shown in Fig. S1b† as follows: around 3300 cm^{-1} a peak for N–H stretching, at 2900 cm^{-1} the one for C–H stretching and at 1463 cm^{-1} that of the N^+-CH_3 bending vibration peak are observed. Moreover, a strong double bond monosubstituted bending absorption peak can be observed between 1000 and 900 cm^{-1}, confirming again the chemical structure of the protic monomer.

Once the protic ionic liquid monomer was obtained, the subsequent step consisted of the polymerization of the protic $DAMAH^+Cl^-$ monomer. It is known that diallyl ammonium monomers polymerize through a cyclopolymerization mechanism using radical initiators.[40,41] The particular mechanisms and polymerization conditions for similar diallyl methylamines and their protonated forms were studied before using a radical photinitiator.[42] During the second step in Scheme 1a, a free radical thermal polymerization process was carried out initiated by 2,2′-azobis(2-methylpropionamidine)dihydrochloride (AIBA). The reaction was conducted *via* inverse emulsion polymerization in water where an aqueous mixture of $DAMAH^+Cl^-$, AIBA, and water was added dropwise to an organic solution of two surfactants, Span 83 and Tween 40, dissolved in the organic solvent, Isopar L. After homogenizing the emulsion, the solution underwent deoxygenation for 30 min and reacted overnight under stirring at 65 °C. The monomer consumption and poly($DAMAH^+Cl^-$) synthesis were confirmed *via* ^1H NMR in *d*-DMSO where the disappearance of typical monomer signals around 5.5 and 6 ppm from the vinylic groups and the appearance of new signals corresponding to the polymer backbone can be observed, as demonstrated in Scheme 1c. A 90% yield conversion was obtained

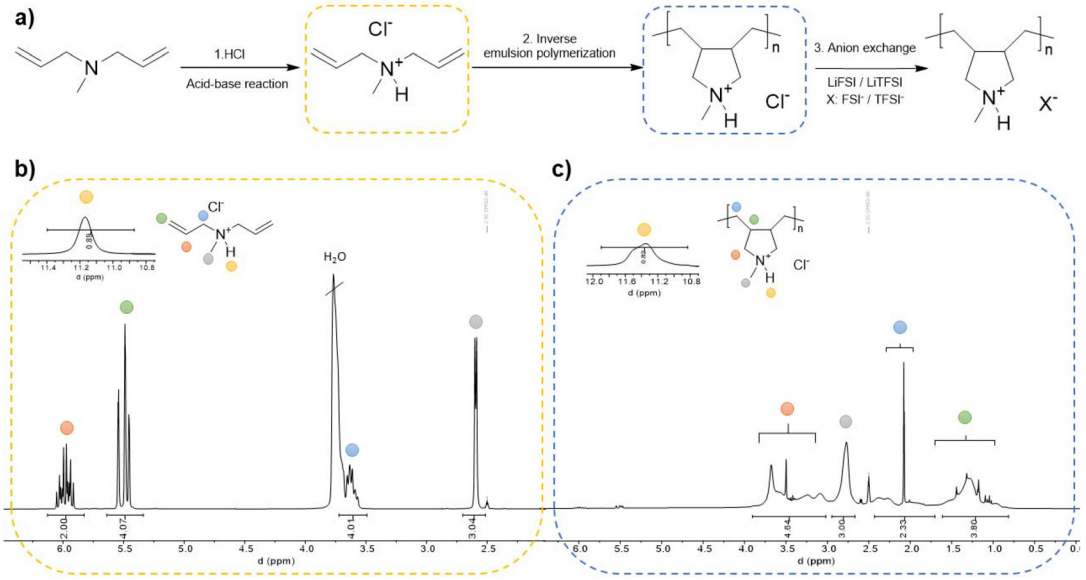

Scheme 1 Synthesis procedure of the protic monomer and the latter inverse emulsion polymerization (a), ^{1}H NMR spectra of the protic monomer (b) and the protic polymer (c).

from the NMR spectrum. Additional signals, like the cyclic structure of the cationic backbone, appear between 1 and 2.5 ppm, while the signals belonging to the methylenes beside the nitrogen moved to a higher field at around 3 and 4 ppm. A minor up-field shift and a wider signal of the H^+ proton between 11.2 and 11.6 ppm can also be noticed in Scheme 1c. Finally, in order to eliminate the surfactants and possible remaining monomer and initiator, the polymer was precipitated in acetone, a step repeated three times to ensure the polymer's purity.

The following and last step was the typical anion exchange reaction used for the synthesis of poly(ionic liquid)s (step 3 in Scheme 1a), carried out in aqueous media. Poly(DAMAH$^+$Cl$^-$) was dissolved in water and lithium bis(fluorosulfonyl)imide (LiFSI) was added in a molar ratio of 1 : 1.2 incrementally with stirring to exchange the anion Cl^- and form the new protic poly(ionic liquid), poly(DAMAH$^+$FSI$^-$), as a white precipitate. The precipitate was redissolved in acetone and dried in an oven at 60 °C for 24 h. The same procedure was carried out with lithium bis(trifluoromethanesulfonyl)imide (LiTFSI) to obtain the second protic poly(DAMAH$^+$TFSI$^-$). After drying the protic poly(ionic liquid)s, size exclusion chromatography (SEC) in THF was carried out to determine the molecular weights and dispersity obtained for the materials. As observed in Fig. S2,† poly(DAMAH$^+$TFSI$^-$) and poly(DAMAH$^+$FSI$^-$) presented an apparent M_w of 37.3k and a relatively low polydispersity of 1.65, while poly(DAMAH$^+$FSI$^-$) showed a M_w of 35.4k and a polydispersity of 1.32.

Molecular mobility and interactions of the protic polymers were examined at the molecular level using solid-state NMR techniques in order to compare the influence of anions. ^{1}H static solid-state NMR single pulse excitation (SPE) spectra of both protic poly(ionic liquid)s can be observed in Fig. 1a. Broad ^{1}H SPE NMR spectra are observed for poly(DAMAH$^+$TFSI$^-$) and poly(DAMAH$^+$FSI$^-$) at 110 °C, indicating a slow molecular mobility, an expected behaviour for neat polymers. ^{1}H NMR signals for both polymers include contributions from the protic cation and the polymer backbone as confirmed later by ^{1}H pulse field gradient (PFG) NMR, a technique normally employed to investigate the diffusion behaviour of different species into, in this case, our protic poly(ionic liquid)s. ^{1}H diffusion of the dry protic polymers could only be determined at 110 °C due to the short T_2's as well as the slow diffusion, ensuring this way an anhydrous environment. From the fitting of the NMR signal attenuation curve, both protic polymers gave, as mentioned before, two diffusion coefficients: poly(DAMAH$^+$TFSI$^-$) presented a diffusion contribution of 2.8 × 10^{-12} m^2 s^{-1} (28%) from labile H^+ and 2.3 × 10^{-13} m^2 s^{-1} (72%) from the polymer backbone, while poly(DAMAH$^+$FSI$^-$) presented, at the same temperature, diffusion values of 4 × 10^{-12} m^2 s^{-1} (83%) from labile H^+ and 6.3 × 10^{-14} m^2 s^{-1} (17%) from the polymer. Poly(DAMAH$^+$FSI$^-$) presented a higher contribution and diffusion coefficient of the labile protic part than its neighbor $TFSI^-$ at high temperatures, which agrees with the local dynamics when compared with the bistriflimide.

In order to observe the anion's influence under hydrated conditions on protic poly(DAMAH$^+$), the same samples inside the rotors employed for dry ^{1}H diffusion were exposed to a relative humidity of 75% during 12 h and analyzed by ^{1}H PFG NMR from 30 to 100 °C, as observed in Fig. 1b. We observed a water uptake of 0.5 wt% for poly(DAMAH$^+$TFSI$^-$) and 0.7 wt% for poly(DAMAH$^+$FSI$^-$) with respect to the dry protic polymer. This low but key hydration allowed the measurement of ^{1}H diffusion coefficients from both the labile proton and the polymer backbone contributions. Over the entire range of

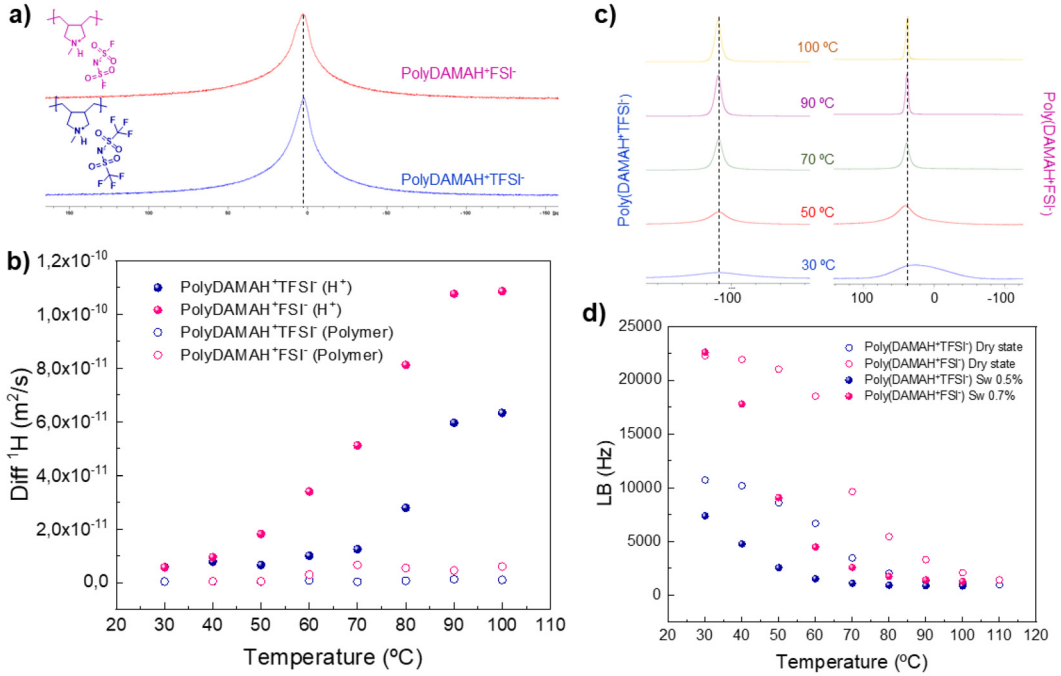

Fig. 1 ^{1}H SPE NMR spectra for poly(DAMAH^{+}TFSI^{-}) and poly(DAMAH^{+}FSI^{-}) at 110 °C in the dry state (a); diffusion coefficients of both protic poly (ionic liquid)s by ^{1}H PFG NMR obtained under 75 RH% from 30 to 100 °C (b); ^{19}F SPE NMR spectra of both protic poly(ionic liquid)s under 75 RH% from 30 to 100 °C (c); and line broadening (LB) comparison between dry and swelled states (d).

temperature, the water uptake influenced the diffusion of both species, with a greater impact on poly(DAMAH^{+}FSI^{-}): the hydrogen polymer diffusion increased one order of magnitude up to 6.3 × 10^{-12} m^{2} s^{-1} (see hollow circles) and the protic H^{+} (full circles) diffusion coefficient up to 1.2 × 10^{-10} m^{2} s^{-1} at 100 °C. FSI^{-} influence on the protic poly(ionic liquid) observed in the figure suggests that the proton contribution on the diffusion measurements will present a higher ionic conductivity and proton mobility *versus* TFSI^{-} at all temperature ranges and under dry or humid conditions.

It is important to highlight that ^{19}F PFG NMR could not be measured in dry or hydrated states, meaning possibly that ^{19}F moves much slower than ^{1}H, even under humid conditions, making H^{+} from the protic backbone the main protagonist of the ion mobility behaviour. Even if ^{19}F PFG NMR could not be measured, solid-state ^{19}F SPE NMR was carried out in order to evaluate the ^{19}F signal line broadening when both protic poly (ionic liquid)s were heated under dry and humid conditions. ^{19}F signal appears normally between −50 and −100 ppm for TFSI^{-} species and around 40 ppm for FSI^{-} ones. Fig. 1c shows that when the temperature increases, the line width narrows slightly more for the FSI^{-} peak in contrast to TFSI^{-}, and that FSI^{-} protic poly(ionic liquid) presents a faster narrowing than TFSI^{-} with temperature due to a faster molecular mobility. From the intersection of the tangents of the curves at lower temperatures, rigid lattice limit and the rapid line narrowing region, we can identify the onset of polymer and/or ion dynamics which is associated with the glass transition temperatures (T_g), being ≈51 °C for poly(DAMAH^{+}FSI^{-}) and ≈49 °C for poly(DAMAH^{+}TFSI^{-}).

Next, a solvent-casting process was carried out in order to obtain poly(DAMAH^{+}TFSI^{-}) and poly(DAMAH^{+}FSI^{-}) protic membranes and evaluate them for further studies. For this, both homopolymers were dissolved in ACN and later poured into silicone molds, allowing the solvent to evaporate overnight under the fume hood. Subsequently, the resulting membranes were subjected to thermal drying in an oven at 60 °C under vacuum for 4 h to ensure complete removal of the residual solvent. After obtaining the membranes, a marked difference in their manageability was observed: poly (DAMAH^{+}TFSI^{-}) membranes exhibited high fragility, being too brittle and difficult to handle, while poly(DAMAH^{+}FSI^{-}) showed a soft and sticky texture, with high flexibility to touch, as observed for both kinds of protic polymers in Fig. S3.† Considering these differences and with the aim of improving the handleability properties with the intention to achieve self-standing membranes, it was decided to carry out a blending procedure of both protic homopolymers in different molar proportions to analyze the behavior of the resulting protic blends. The results were encouraging, as the membranes produced through the solvent-casting process demonstrated significant improvements in their mechanical properties as they were easier to manipulate. As detailed in Fig. 2a, during the mixing process, poly(DAMAH^{+}TFSI^{-}) and poly(DAMAH^{+}FSI^{-}) homopolymers were dissolved in ACN and mixed in molar ratios of 2 : 1, 1 : 1, and 1 : 2, generating in this way, five protic mem-

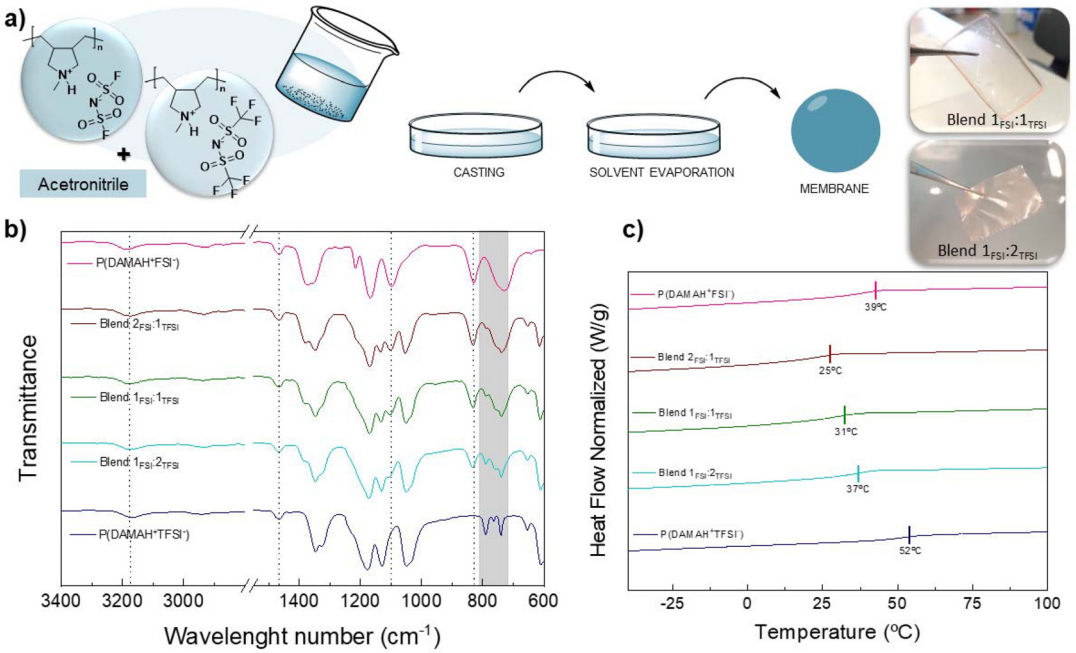

Fig. 2 Blending scheme formation (a), FTIR spectra (b) and DSC (c) characterization of all protic membranes.

branes along with the protic homopolymers. For their further characterization and comparison, the new protic membranes were named: Blend $2_{FSI}:1_{TFSI}$, Blend $1_{FSI}:1_{TFSI}$ and Blend $1_{FSI}:2_{TFSI}$. Fig. 2a shows pictures of Blend $1_{FSI}:1_{TFSI}$ and Blend $1_{FSI}:2_{TFSI}$, both of them completely transparent and easy to handle and prepared by the same procedure mentioned before.

FTIR spectra were analyzed in order to study the chemical structure of all protic membranes and also to evaluate how the contribution of both anions affects the ion–ion interaction in different blends. The spectra collected for protic homopolymers and blends can be seen in Fig. 2b. The most characteristic signal corresponding to the protic cation backbone side is the stretching vibration one of N–CH_3 which appears at around 1465 cm^{-1}. The stretching signal of SO_2 corresponding to the FSI anion is present at 1100 cm^{-1}, where a decrease in the intensity of this signal can be observed as the amount of poly(DAMAH$^+$FSI$^-$) contribution decreases in the blend. The same behavior occurs with the asymmetric vibration signal corresponding to the S–N–S group at 830 cm^{-1}. TFSI anion is mainly recognized by a particular doublet molecular vibration band corresponding to the cationic interaction between in this case DAMAH$^+$ and the anion[37] in the region of 740–800 cm^{-1}. The vibrations associated with the N–H protic poly(ionic liquid)s can be observed in the range of 3000–3400 cm^{-1}, where poly(DAMAH$^+$FSI$^-$) presents the peak at 3186 cm^{-1}, while poly(DAMAH$^+$TFSI$^-$) presents it at a lower wavelength number of 3168 cm^{-1}. This difference can be explained by taking into account the interaction of each anion with the cationic backbone: FSI might interact less with the cationic N–H than TFSI, meaning that the stretching vibration requires more energy, shifting to higher wavenumbers; while TFSI interacts more than FSI through hydrogen bonding, decreasing the energy required for the stretching vibration of N–H and leading to a shift to lower wavenumbers. This effect observed in Fig. 2b supports the result of ^{1}H SPE NMR shown in Fig. 1, where it was shown that the FSI anion promotes higher proton mobility than TFSI$^-$. The blends present an N–H vibration at around 3175 cm^{-1}, a middle point between the protic homopolymers analyzed.

DSC analysis was also carried out to study the T_g of each protic membrane. As it can be observed in Fig. 2c, and previously reported, pure poly(DAMAH$^+$FSI$^-$) shows a T_g of approximately 39 °C while poly(DAMAH$^+$TFSI$^-$) presents a T_g of around 52 °C, close values to the ones estimated from the solid-state ^{19}F SPE NMR measurements, as previously mentioned (51 °C for poly(DAMAH$^+$FSI$^-$) and 49 °C for poly (DAMAH$^+$TFSI$^-$)). The T_g for the protic homopolymers are notably lower than the previously reported T_g of the aprotic polymer, $T_g \approx 121$ °C for poly(DADMA)FSI[43] and $T_g \approx 116$ °C for poly(DADMA)TFSI.[44,45] This lower T_g in the case of the protic poly(ionic liquid)s indicates the internal plasticizing effect of the protic *versus* the alkyl substituent, highlighting the role played by the proton. Focusing on the blends, surprisingly a lower T_g than the ones obtained for the protic homopolymers can be noticed, being ≈25 °C for Blend $2_{FSI}:1_{TFSI}$, ≈ 31 °C for Blend $1_{FSI}:1_{TFSI}$ and ≈37 °C for Blend $1_{FSI}:2_{TFSI}$. This negative deviation of T_g from linear behaviour in polymer blends is often observed and can be explained by the presence of intermolecular bonds that increase the effective free volume in the blend, leading to the reduction in the cohesive energy density, thereby lowering the glass transition temperature.[46]

Thermal stability is an important parameter to understand the temperature range application of these protic materials. For this reason, the thermal stability profile of all protic poly (ionic liquid)s and their starting degradation temperature can be seen in Fig. S4.† Poly(DAMAH$^+$FSI$^-$) shows the lowest degradation temperature value around 250 °C when a 5 wt% degradation takes place. On the other hand, poly(DAMAH$^+$TFSI$^-$) presents the highest degradation temperature with a value near 400 °C for 5 wt% weight loss. Comparing these values with those of the aprotic version previously reported,[43] a minor decrease in the degradation temperature can be observed. In the case of the blends, thermal stability slightly increases as the amount of poly(DAMAH$^+$TFSI$^-$) increases, although in any case the degradation temperature observed is around 260 °C when 5 wt% weight loss takes place. Interestingly, the protic poly(ionic liquid)s were thermally stable at around 120 °C which is an interesting temperature for application of intermediate temperature PEMFCs.

Characterization of the protic poly(ionic liquid) membranes

The determination of the protic polyDAMAH FSI/TFSI membrane properties in terms of ionic conductivity, water uptake and mechanical behaviour is a key study for its evaluation as proton exchange membranes. Fig. 3 shows the measurement of the ionic conductivity through electrochemical impedance spectroscopy (EIS) analysis under dry and different relative humidity (RH) conditions for the protic membranes. After drying under vacuum at 60 °C (RH 0%), Fig. 3a presents the tendency found for all protic poly(ionic liquid)s at 30, 50, 80 and 100 °C: the highest values of ionic conductivity belong to poly(DAMAH$^+$FSI$^-$) at 4×10^{-4} S cm^{-1} at 100 °C, while that of poly(DAMAH$^+$TFSI$^-$) could only be measured at 100 °C due to the brittleness of the sample, giving a value of 3.7×10^{-7} S cm^{-1}, differing by almost three orders of magnitude which can be considered as a big difference taking into account the similarity in the anion chemical structure. Taking into account the cationic polymer backbone structure, the value of ionic conductivity of 1.63×10^{-4} S cm^{-1} at 70 °C for poly(DAMAH$^+$FSI$^-$) is three orders of magnitude higher than the one reported for the aprotic version poly(DADMA)FSI,[43] highlighting again the great effect that the proton produces for the mobility of ion species compared to the methyl group. It can also be noticed that when both protic polymers are mixed in different molar ratios, the ionic conductivity increases as the amount of poly (DAMAH$^+$FSI$^-$) increases in the blend, an expected behaviour due to the presence of FSI that already demonstrated by ^{1}H PFG NMR a higher diffusion coefficient for the protic species.

Ionic conductivity was also measured by EIS under three different conditions, 30%, 50%, and 75% of RH, this last condition is observed in Fig. 3b. For this study, a previous water

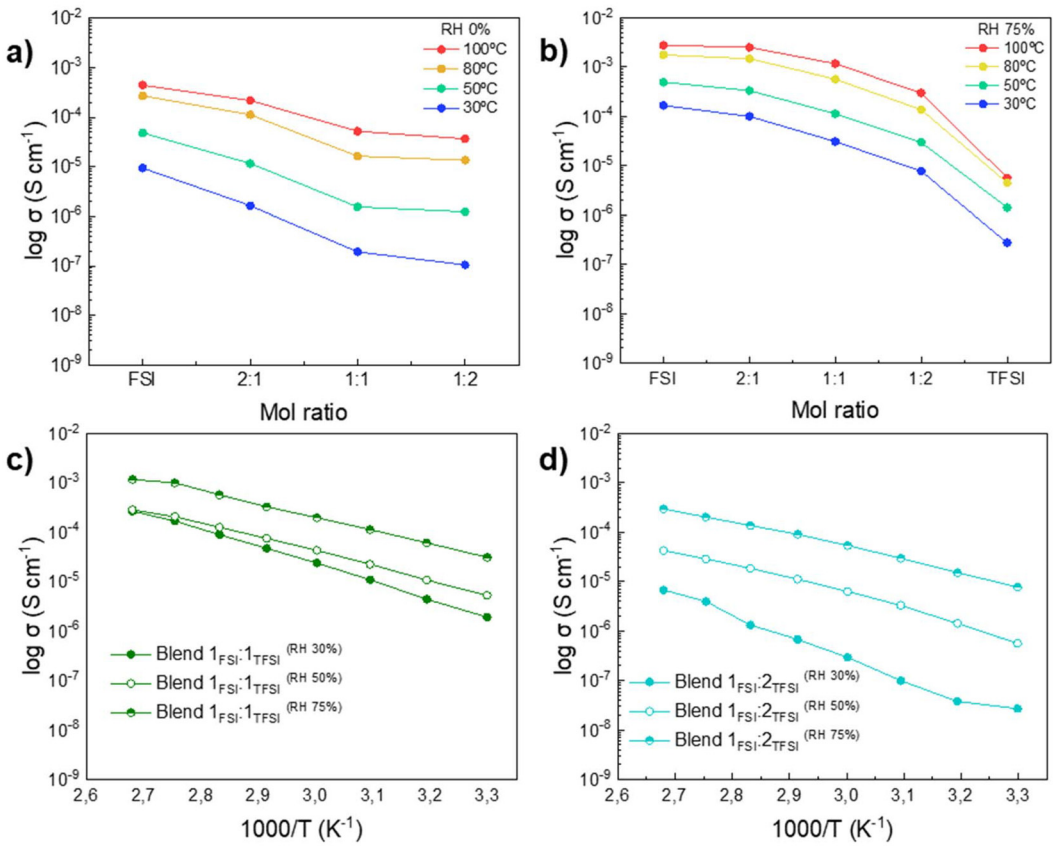

Fig. 3 Ionic conductivity measurements by electrochemical impedance spectroscopy (EIS) under dry (a) and 75% RH conditions at 30, 50, 80 and 100 °C (b) of all protic membranes; and ionic conductivity comparison between different RH% of Blend 1$_{FSI}$: 1$_{TFSI}$ (c) and Blend 1$_{FSI}$: 2$_{TFSI}$ (d).

uptake analysis was carried out: all protic membranes were exposed to the mentioned conditions during three days at room temperature, checking the weight gain after the determined time. In Fig. S6† the percentage of water uptake for each sample after the exposure to the three RH conditions can be seen. The protic homopolymer poly(DAMAH$^+$FSI$^-$) presented the highest percentage under all conditions, being 6.5% water absorption at 75% RH. While on the other hand, even if poly(DAMAH$^+$TFSI$^-$) presented lower water uptake (WU) under all RH conditions compared to poly (DAMAH$^+$FSI$^-$), the blends containing FSI surprisingly did not increase the WU% (all of them between 1 and 3% WU), all values being similar to the TFSI protic membrane.

An increase in the ionic conductivity of the protic membranes is observed as the temperature and relative humidity increase; a behavior that can be noticed by comparing Fig. 3a, b and Fig. S7a, b.† This linear temperature dependence of the ionic conductivity indicates that the ion transport is thermally activated. The increase of ionic conductivity that results from the increase in temperature is a well-known phenomenon, correlated with the vibrational energy of the segmental motion of the polymer chains that creates free volume around them, thereby facilitating ion mobility, favoring inter- and intrachain ion hopping and ultimately enhancing the ionic conductivity of the membranes. Moreover, the increase of ionic conductivity as a function of temperature and RH may be also associated with a decrease in the T_g of the poly(ionic liquid) and the concomitant increase in chain flexibility.[39]

Under all the studied conditions, the most conductive membrane is the homopolymer poly(DAMAH$^+$FSI$^-$) followed by Blend 2 : 1, Blend 1 : 1, Blend 1 : 2, and finally poly (DAMAH$^+$TFSI$^-$). The activation energy (E_a) was also calculated for dry and 75% RH states. E_a is an important parameter since it is associated with the potential barrier to be overcome for an ion to move thanks to the dynamics of the polymer, the ion 'hop' from one site to another in the polymer, plus the energy required to deform the polymer structure to allow ion migration.[39] As can be seen in Table S1,† the reduction of the E_a values with the increment of RH was expected: the higher the relative humidity the more 'plasticized' the polymer becomes making it easier for the ions to move. On analyzing the E_a values of the five samples in dry and 75% RH states, it can be noticed that the protic homopolymers present lower E_a values when compared with the blends.

As an example, a comparison of 30, 50 and 75 RH% of Blend $1_{FSI} : 1_{TFSI}$ and Blend $1_{FSI} : 2_{TFSI}$ can be seen in Fig. 3c and d. These results show the enhancement of the ionic conductivity with the increase of relative humidity and temperature for both protic membranes, Blend $1_{FSI} : 1_{TFSI}$ being the best one in terms of ionic conductivity values. In the absence of any additional compounds that may augment conductivity, the observed results demonstrate notable performance and competitiveness in comparison to Nafion 117, the currently preferred material for proton exchange membranes in contemporary applications. As elucidated before,[47] the recorded ionic conductivity values of Nafion 117 at RH values of 34%, 53%, and 73% at 30 °C are 1.4×10^{-4}, 7.7×10^{-4}, and 3.4×10^{-3} S cm^{-1}, respectively. In the case of the Blend $1_{FSI} : 1_{TFSI}$, the corresponding ionic conductivity measurements at the same temperature (1.9×10^{-6}, 5.2×10^{-6}, and 3.1×10^{-5} S cm^{-1}) were attained under identical conditions of RH and temperature. However, at intermediate temperatures targeted in this work, Nafion shows a decrease in conductivity in the absence of humidification, these new protic materials exhibit a conductivity of 1.2×10^{-3} S cm^{-1} at 100 °C which brings these materials in the proximity to Nafion at lower temperatures and high humidity. Blend $1_{FSI} : 2_{TFSI}$ ionic conductivity results shown in Fig. 3d are not as promising as those of Blend $1_{FSI} : 1_{TFSI}$ but it could be also considered a protic membrane for supplanting Nafion 117 in high-temperature proton exchange membranes for fuel cells due to its hydrophobicity and good handling properties.

The most promising membranes are Blend $1_{FSI} : 1_{TFSI}$ and Blend $1_{FSI} : 2_{TFSI}$ due to their good combination of membrane properties and ionic conductivity. Due to this, mechanical properties were analyzed by DMTA at 75% RH, as shown in Fig. 4a, considering also that both protic membranes achieve similar WU% (2.8 and 2% for Blend $1_{FSI} : 2_{TFSI}$ and Blend $1_{FSI} : 1_{TFSI}$). We found that, at 1 Hz and 25 °C, Blend $1_{FSI} : 2_{TFSI}$ presented a storage modulus of 1.1×10^5 Pa, while for Blend $1_{FSI} : 1_{TFSI}$ 4.4×10^5 Pa was obtained. When increasing the temperature to 80 °C, the storage moduli were now inverted with blend Blend $1_{FSI} : 1_{TFSI}$ having a higher value of 2.2×10^5 Pa and Blend $1_{FSI} : 2_{TFSI}$ with a value of 1×10^5 Pa at 1 Hz. Fig. 4b presents strain–stress curves for both blends at 25 °C and 75% RH: Blend $1_{FSI} : 2_{TFSI}$ showed a higher tensile strength and a lower elongation at break, typical of brittle materials, whereas the Blend $1_{FSI} : 1_{TFSI}$ membrane had more ductile behaviour, capable of absorbing more energy before fracture. Mechanical properties, measured by DMTA and stress–strain curves, suggested that a FSI : TFSI molar ratio of 1 : 1 is the best candidate for proton exchange membranes. Pictures of Blend $1_{FSI} : 1_{TFSI}$ are shown in Fig. 4c (75% RH at room temperature) indicating high flexibility, with facile stretching and bending of the protic membrane and retention of its physical form.

Finally, the ion dynamics of a Blend $1_{FSI} : 1_{TFSI}$ over a wide temperature range will be discussed. For this purpose, the dielectric and mechanical measurements were performed. The former follows the charge transport, while the latter provides information about the segmental dynamics of the examined $1_{FSI} : 1_{TFSI}$ blend. Fig. 5a and b show the representative dielectric results in the electric modulus and conductivity formalisms, respectively. As can be seen, the imaginary part of complex modulus $M''(f)$ takes the form of a well-resolved peak, so-called conductivity relaxation (denoted as a σ-process), that shifts toward lower frequencies as the temperature decreases. At the same time, the real part of complex conductivity $\sigma'(f)$ reveals three characteristic regions: (i) frequency-independent part, usually denoted as dc-conductivity σ_{dc}, that is proportional to the number of ions and their mobility, (ii) low-frequency decrease of σ' reflecting electrode polar-

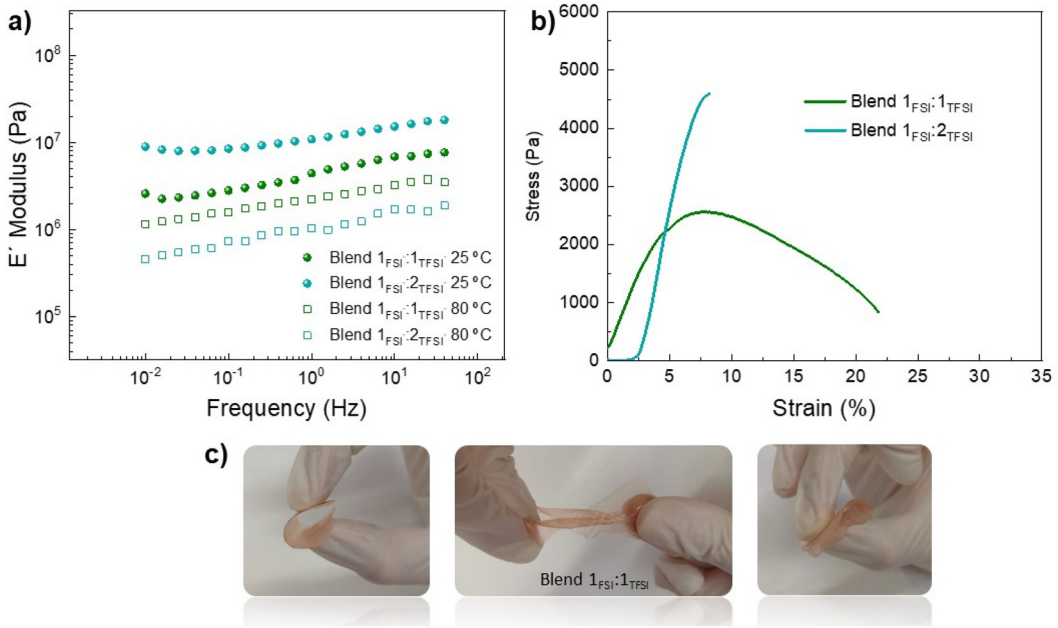

Fig. 4 DMTA frequency scan at 1% strain and at 25 and 80 °C (a); stress–strain curves at 25 °C for protic Blend $1_{FSI}:1_{TFSI}$ and Blend $1_{FSI}:2_{TFSI}$ at 25 °C and 75% RH (b); and pictures of Blend $1_{FSI}:1_{TFSI}$ at 75% RH (c).

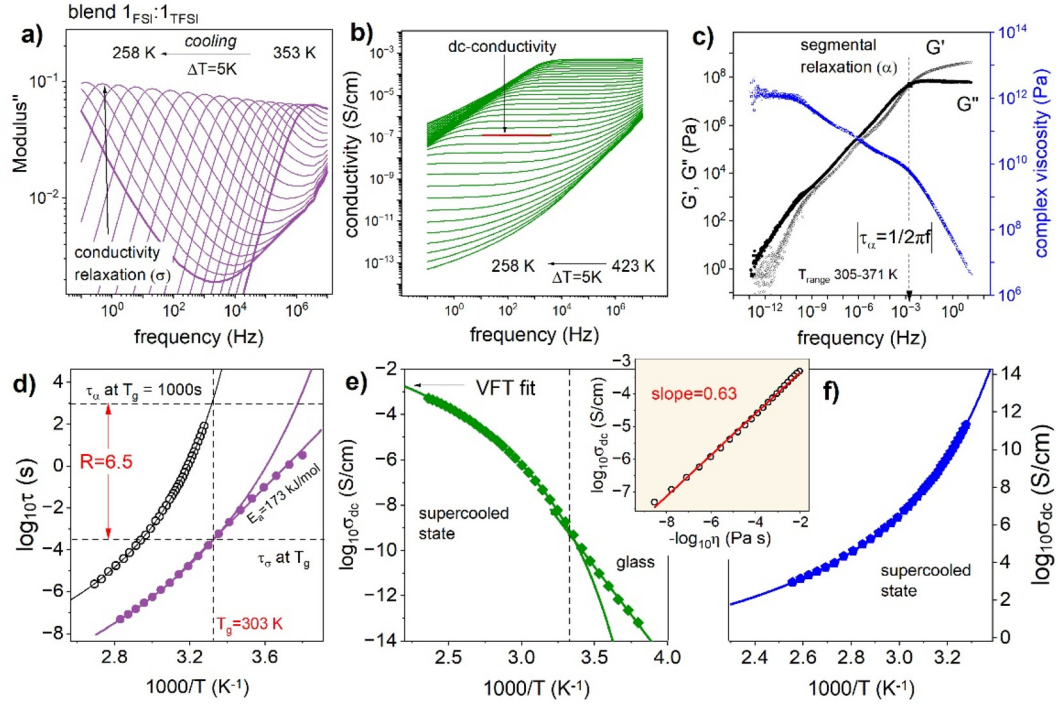

Fig. 5 Dielectric and mechanical response of examined blend $1_{FSI}:1_{TFSI}$: imaginary part of the complex electric modulus M'' (a) and real part of complex conductivity σ' as a function of frequency at various temperatures (b); storage, loss modulus, and complex viscosity of the $1_{FSI}:1_{TFSI}$ blend presented in the form of mastercurve (c); temperature dependence of conductivity (closed circles) and segmental (open circles) relaxation times (d); temperature dependence of dc-conductivity (e) and viscosity (f) are analyzed together in the form of a Walden plot (inset).

ization, and (iii) a power-law behavior obeyed on the high-frequency side. Note that the dc-conductivity plateau is well visible even up to 423 K, while the modulus peak maximum moves out of the experimental frequency window already above 353 K. Consequently, the temperature dependence of σ_{dc} over 10 orders of magnitude of frequency can be examined. At

the same time, the conductivity relaxation time τ_σ (defined as the inverse of M'' peak maximum ($\tau_\sigma = 1/2\pi f_{max}$)) behavior can be monitored over 7 decades. To provide more detailed information about the ion mobility in the $1_{FSI}:1_{TFSI}$ blend, the temperature behavior of dc-conductivity σ_{dc} and conductivity relaxation times τ_σ are plotted in Fig. 5d and e. As can be seen, the experimental data deviate from the high-temperature Arrhenius law, which is typical.[48] Therefore, the Vogel–Fulcher–Tammann equation $\tau_\sigma(T) = \tau_\infty \exp\left(\frac{DT_0}{T - T_0}\right)$ has been used to parameterize the $\log \sigma_{dc}(1000/T)$ and $\log \tau_\sigma(1000/T)$ dependencies in the supercooled state down to T_g. On the other hand, close to the calorimetric T_g, a clear crossover from VFT to linear behavior is visible. According to the reports on protic ionic conductors, the observed crossover manifests the liquid-to-glass transition of the examined 1 : 1 blend and suggests decoupling between the charge transport and segmental dynamics.[49,50]

The latter statement comes from the fact that T_g is usually defined as the temperature at which the structural relaxation time, or segmental relaxation time in the case of polymers, τ_α, is equal to 10^3 s.[51] However, the kink of the $\tau_\sigma(T)$ curve obtained for a 1 : 1 blend occurs at much shorter conductivity relaxation times ($\log \tau_\sigma \sim -3.5$). To explore the relation between charge transport and segmental relaxation in a $1_{FSI}:1_{TFSI}$ blend in more detail, mechanical measurements were performed. The dynamic shear loss and storage modulus, denoted as G'' and G' respectively, are shown in Fig. 5c as master curves constructed using the time–temperature superposition (TTS) rule. The shear modulus relaxation times τ_α of the $1_{FSI}:1_{TFSI}$ blend were calculated directly from the frequency denoting G'' and G' intersection, which corresponds well to the $G''(f)$ peak maximum and plotted in Fig. 5d. As can be easily seen in Fig. 5d, at the conductivity relaxation time T_g, describing the ion's migration through the polymer matrix is 6.5 decades faster than its segmental relaxation time. It means that the ions (in this case, protons and anions) might still diffuse when the segmental dynamics are very slow or completely frozen below T_g. Importantly, the time scale separation between τ_σ and τ_α is also visible when the conductivity and viscosity are analyzed together in terms of the modified Walden rule, $\sigma_{dc}\eta^{-k}$ = const. The inset shows dc-conductivity *vs.* fluidity on a double logarithmic scale. As presented, the fractional exponent k is significantly lower than unity (k = 0.63) for the examined $1_{FSI}:1_{TFSI}$ blend, that again confirms fast charge transport independent of segmental dynamics in the examined system.

Conclusions

This article presents an innovative family of proton exchange membranes (PEMs) based on protic poly(diallylmethylammonium) (PDAMAH) through a simple synthesis route, eliminating the need for toxic polyfluoroalkyl substances (PFSAs). These novel membranes, incorporating sulfonamides like TFSI and FSI as counter-ions, demonstrate substantial enhancements in mechanical properties, membrane formation, and thermal stability while maintaining minimal water uptake, between 1.5 and 3 wt%, at all evaluated relative humidities. They exhibited glass transition temperatures between 25 °C and 52 °C for the different homopolymers and blends. The optimized PDAMAH membranes achieved a high ionic conductivity of 1.2×10^{-3} S cm^{-1} at 100 °C and 75% relative humidity, along with a storage modulus exceeding 1×10^6 Pa and great manageability. These findings indicate that protic PDAMAH membranes are a promising and more environmentally friendly alternative for green hydrogen technologies, such as electrolyzers and fuel cells, marking a significant step forward in developing safer and more sustainable solutions in the renewable energy sector.

Data availability

The authors confirm that the data supporting the findings of this study are available within the article [and/or] its ESI.†

Conflicts of interest

There are no conficts to declare.

Acknowledgements

Financial support from the Horizon Europe Program (IONBIKE 2.0 MSCA-SE 101129945), the Basque Government (GV-KK-2024-00035) and MINECO AEI (PID2023-153050OB-I00) is gratefully acknowledged. MF acknowledges support from the Australian Research Council through the ARC Industry Transformation Training Centre for Future Energy Storage Technologies (storEnergy) through IC180100049. I. Abdel Aziz acknowledges the funding from the European Union's Horizon 2020 Research and Innovation Programme under the Marie Skłodowska-Curie grant agreement No 101034379.

References

1 L. Fan, Z. Tu and S. H. Chan, *Energy Rep.*, 2021, **7**, 8421–8446.
2 B. G. Pollet, S. S. Kocha and I. Staffell, *Curr. Opin. Electrochem.*, 2019, **16**, 90–95.
3 P. E. Dodds, I. Staffell, A. D. Hawkes, F. Li, P. Grünewald, W. McDowall and P. Ekins, *Int. J. Hydrogen Energy*, 2015, **40**, 2065–2083.
4 H. Kahraman and Y. Akın, *Energy Convers. Manage.*, 2024, **304**, 118244.
5 S. Mo, L. Du, Z. Huang, J. Chen, Y. Zhou, P. Wu, L. Meng, N. Wang, L. Xing, M. Zhao, Y. Yang, J. Tang, Y. Zou and S. Ye, *Electrochem. Energy Rev.*, 2023, **6**, 28.

6 M. Adamski, N. Peressin and S. Holdcroft, *Mater. Adv.*, 2021, **2**, 4966–5005.
7 H. Zhang and P. K. Shen, *Chem. Rev.*, 2012, **112**, 2780–2832.
8 R. Haider, Y. Wen, Z.-F. Ma, D. P. Wilkinson, L. Zhang, X. Yuan, S. Song and J. Zhang, *Chem. Soc. Rev.*, 2021, **50**, 1138–1187.
9 R. E. Rosli, A. B. Sulong, W. R. W. Daud, M. A. Zulkifley, T. Husaini, M. I. Rosli, E. H. Majlan and M. A. Haque, *Int. J. Hydrogen Energy*, 2017, **42**, 9293–9314.
10 T. K. Maiti, J. Singh, J. Majhi, A. Ahuja, S. Maiti, P. Dixit, S. Bhushan, A. Bandyopadhyay and S. Chattopadhyay, *Polymer*, 2022, **255**, 125151.
11 S. Cong, J. Wang, Z. Wang and X. Liu, *Green Chem. Eng.*, 2021, **2**, 44–56.
12 Y. Oono, A. Sounai and M. Hori, *J. Power Sources*, 2009, **189**, 943–949.
13 S. Kaserer, K. M. Caldwell, D. E. Ramaker and C. Roth, *J. Phys. Chem. C*, 2013, **117**, 6210–6217.
14 Y. Hu, Y. Jiang, J. O. Jensen, L. N. Cleemann and Q. Li, *J. Power Sources*, 2018, **375**, 77–81.
15 A. Alashkar, A. Al-Othman, M. Tawalbeh and M. Qasim, *Membranes*, 2022, **12**, 178.
16 L. Sun, S. Qu, X. Lv, J. Duan and W. Wang, *J. Appl. Polym. Sci.*, 2023, **140**(4), e53384.
17 T. K. Maiti, P. Dixit, J. Singh, N. Talapatra, M. Ray and S. Chattopadhyay, *Int. J. Hydrogen Energy*, 2023, **48**, 1482–1500.
18 X. Wang, M. Jin, Y. Li and L. Zhao, *Electrochim. Acta*, 2017, **257**, 290–300.
19 T. L. Greaves and C. J. Drummond, *Chem. Rev.*, 2015, **115**, 11379–11448.
20 J. Stoimenovski, E. I. Izgorodina and D. R. MacFarlane, *Phys. Chem. Chem. Phys.*, 2010, **12**, 10341.
21 M. S. Gruzdev, L. E. Shmukler, N. O. Kudryakova, A. M. Kolker, Y. A. Sergeeva and L. P. Safonova, *J. Mol. Liq.*, 2017, **242**, 838–844.
22 H. A. Elwan, M. Mamlouk and K. Scott, *J. Power Sources*, 2021, **484**, 229197.
23 T. Stettner and A. Balducci, *Energy Storage Mater.*, 2021, **40**, 402–414.
24 A. Alashkar, A. Al-Othman, M. Tawalbeh and M. Qasim, *Membranes*, 2022, **12**, 178.
25 D. Mecerreyes, *Prog. Polym. Sci.*, 2011, **36**, 1629–1648.
26 A. S. Shaplov, D. O. Ponkratov and Y. S. Vygodskii, *Polym. Sci., Ser. B*, 2016, **58**, 73–142.
27 J. Yuan, D. Mecerreyes and M. Antonietti, *Prog. Polym. Sci.*, 2013, **38**, 1009–1036.
28 V. M. Ortiz-Martínez, A. Ortiz, V. Fernández-Stefanuto, E. Tojo, M. Colpaert, B. Améduri and I. Ortiz, *Polymer*, 2019, **179**, 121583.
29 M. Isik, L. Porcarelli, N. Lago, H. Zhu, M. Forsyth and D. Mecerreyes, *Macromol. Rapid Commun.*, 2018, **39**(3), 1700627.
30 G. Huang, H. Zhu, L. Porcarelli, Y. García, L. A. O'Dell and M. Forsyth, *Macromol. Chem. Phys.*, 2022, **223**(17), 2200124.
31 J. Bailey, E. L. Byrne, P. Goodrich, P. Kavanagh and M. Swadźba-Kwaśny, *Green Chem.*, 2024, **26**, 1092–1131.
32 M. Anouti, M. Caillon-Caravanier, Y. Dridi, H. Galiano and D. Lemordant, *J. Phys. Chem. B*, 2008, **112**, 13335–13343.
33 D. Mecerreyes, *Prog. Polym. Sci.*, 2011, **36**, 1629–1648.
34 C. Karlsson and P. Jannasch, *ACS Appl. Energy Mater.*, 2019, **2**, 6841–6850.
35 J. Wang, Q. Yang, S. Liu, S. Tan, C. Wang and Y. Wu, *Ind. Eng. Chem. Res.*, 2023, **62**, 21977–21985.
36 A. Aslan, S.Ü Çelik, Ü. Şen, R. Haser and A. Bozkurt, *Electrochim. Acta*, 2009, **54**, 2957–2961.
37 A. Gallastegui, F. Foglia, P. F. McMillan, N. Casado, A. Gueguen and D. Mecerreyes, *Polymer*, 2023, **280**, 126064.
38 A. H. Shah, J. Li, H. Yang, U. A. Rana, V. Ranganathan, H. M. Siddigi, D. R. MacFarlane, M. Forsyth and H. Zhu, *J. Mater. Chem. A*, 2016, **4**, 7615–7623.
39 M. Fernandes, M. A. Cardoso, L. C. Rodrigues, M. M. Silva, R. A. S. Ferreira, L. D. Carlos, S. C. Nunes and V. de Zea Bermudez, *J. Electroanal. Chem.*, 2017, **799**, 249–256.
40 A. S. Shaplov, R. Marcilla and D. Mecerreyes, *Electrochim. Acta*, 2015, **175**, 18–34.
41 T. L. Greaves and C. J. Drummond, *Chem. Rev.*, 2008, **108**, 206–237.
42 L. M. Timofeeva, Y. A. Vasilieva, N. A. Kleshcheva and D. A. Topchiev, *Russ. Chem. Bull.*, 1999, **48**, 856–863.
43 R. Del Olmo, N. Casado, J. L. Olmedo-Martínez, X. Wang and M. Forsyth, *Polymers*, 2020, **12**, 1981.
44 R. Yunis, G. M. A. Girard, X. Wang, H. Zhu, A. J. Bhattacharyya, P. Howlett, D. R. MacFarlane and M. Forsyth, *Solid State Ionics*, 2018, **327**, 83–92.
45 G. Huang, L. Porcarelli, Y. Liang, M. Forsyth and H. Zhu, *ACS Appl. Energy Mater.*, 2021, **4**, 10593–10602.
46 M. Mohammadi, H. Fazli, M. Karevan and J. Davoodi, *Eur. Polym. J.*, 2017, **91**, 121–133.
47 A. V. Anantaraman and C. L. Gardner, *J. Electroanal. Chem.*, 1996, **414**(2), 115–120.
48 M. Paluch, *Dielectric Properties of Ionic Liquids*, Springer International Publishing, Cham, 2016.
49 Z. Wojnarowska, Y. Wang, J. Pionteck, K. Grzybowska, A. P. Sokolov and M. Paluch, *Phys. Rev. Lett.*, 2013, **111**, 225703.
50 Z. Wojnarowska, H. Feng, M. Diaz, A. Ortiz, I. Ortiz, J. Knapik-Kowalczuk, M. Vilas, P. Verdía, E. Tojo, T. Saito, E. W. Stacy, N.-G. Kang, J. W. Mays, D. Kruk, P. Wlodarczyk, A. P. Sokolov, V. Bocharova and M. Paluch, *Chem. Mater.*, 2017, **29**, 8082–8092.
51 G. Floudas, M. Paluch, A. Grzybowski and K. L. Ngai, *Molecular Dynamics of Glass-Forming Systems: Effects of Pressure*, Berlin, 1st edn, 2011.

